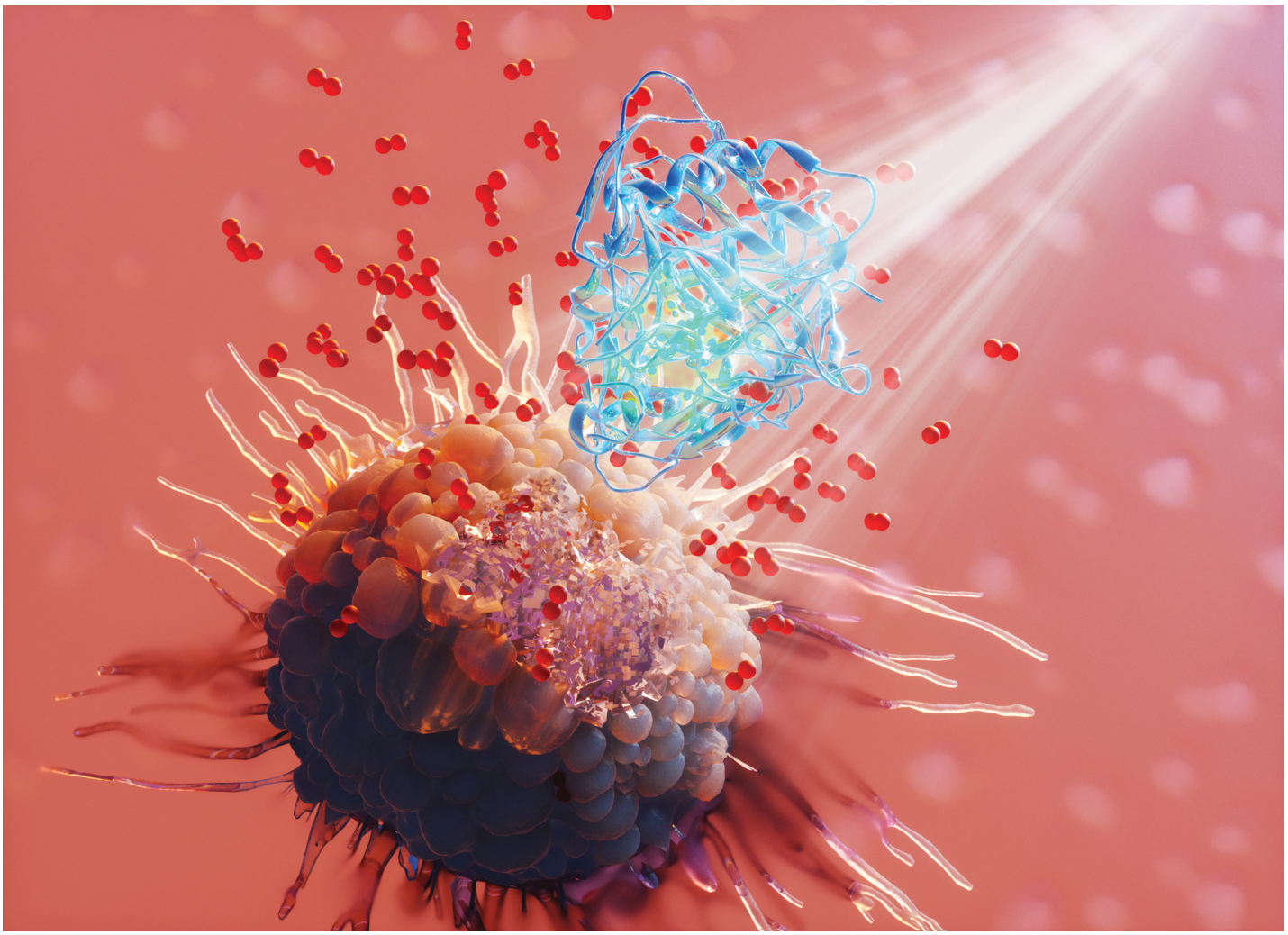

Showcasing research from Professor Sébastien Clément's laboratory, ICGM, Univ Montpellier, CNRS, ENSCM, Montpellier, France and Professor Jean-Yves Winum's laboratory, IBMM, Univ Montpellier, CNRS, ENSCM, Montpellier, France.

Thiochromenocarbazole imide-based photosensitizers decorated with carbonic anhydrase inhibitors for the targeted treatment of hypoxic tumours

Photodynamic therapy (PDT) is promising for cancer treatment due to its low invasiveness and toxicity. However, oxygen levels in tumours affect its effectiveness, especially in hypoxic regions. Thiochromenocarbazole imide (TCI) photosensitizers with carbonic anhydrase inhibitors (CAi) were developed to address this challenge. TCIs with coumarin and sulfocoumarine selectively inhibited tumour-associated hCA IX and hCA XII, enhancing PDT efficiency. Biological assays showed minimal dark toxicity and strong PDT effects, suggesting potential for effective cancer therapy.

As featured in:

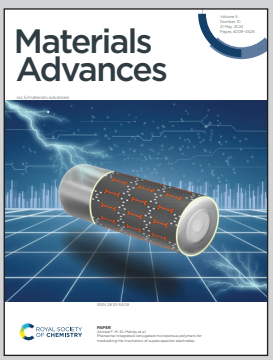

See Jean-Yves Winum, Sébastien Clément *et al.*, *Mater. Adv.*, 2024, **5**, 4172.

ROYAL SOCIETY OF CHEMISTRY

rsc.li/materials-advances

Registered charity number: 207890

Materials Advances

ROYAL SOCIETY OF CHEMISTRY

PAPER

View Article Online
View Journal | View Issue

Cite this: *Mater. Adv.*, 2024, 5, 4172

Thiochromenocarbazole imide-based photosensitizers decorated with carbonic anhydrase inhibitors for the targeted treatment of hypoxic tumours†

Amina Merabti,[ab] Darío Puchán Sánchez,[c] Alessio Nocentini,[d] Lamiaa M. A. Ali,[b] Christophe Nguyen,[b] Denis Durand,[b] Kathleen Hamon,[b] Tatiana Ghanem,[c] Philippe Arnoux,[e] Pierre Josse,[c] Céline Frochot,[e] Raivis Zalubovskis,[f] Sébastien Richeter,[a] Magali Gary-Bobo,[b] Claudiu T. Supuran,[d] Clément Cabanetos,[c] Jean-Yves Winum *[b] and Sébastien Clément *[a]

PDT has gained growing interest as a prospective approach for cancer therapy, thanks to its minimal invasiveness and low systemic toxicity, making it a promising therapeutic option. Nevertheless, type II PDT is significantly influenced by the oxygen levels in the tumoral microenvironment. Consequently, the weak oxygen pressure encountered in hypoxic regions of solid tumours poses a significant challenge in cancer treatment. In this case, PDT efficiency is reduced and the existing hypoxia is intensified by oxygen consumption and vascular closure, activating the angiogenic factors and thus, potentially leading to cancer recurrence and progression. We describe here a series of thiochromenocarbazole imide (TCI) photosensitizers featuring carbonic anhydrase inhibitors (CAi) of the sulfonamide, coumarin and sulfocoumarine type, designed to alleviate the consequences of PDT-induced hypoxia by merging the advantages of hCA IX knockdowns with PDT. TCIs with coumarin and sulfocoumarin moieties showed selective inhibition against tumour-associated hCA IX and hCA XII, while TCI incorporating benzenesulfonamide moieties also showed activity against the off-target hCA II. In biological assays, the TCI photosensitizer incorporating coumarin-based CAi demonstrated minimal dark toxicity and showcased strong imaging and photodynamic therapy (PDT) effects in both *in vitro* and *in vivo* settings.

Received 29th October 2023,
Accepted 8th February 2024

DOI: 10.1039/d3ma00926b

rsc.li/materials-advances

Introduction

Photodynamic therapy (PDT) has emerged as a promising therapeutic approach for solid cancer treatment, due to its minimal invasiveness, high safety and low systemic toxicity.[1,2] A typical PDT process involves the *in situ* formation of cytotoxic reactive oxygen species (ROS) such as singlet oxygen ($^1O_2$), peroxide (O_2^-), superoxide ($O_2^{\bullet -}$) and the hydroxyl radical ($HO^\bullet$) through the photoexcitation of a photosensitizer (PS), accumulated in the tumour, under appropriate light irradiation.[3,4] The PDT process can be categorized into type I and type II depending on the photo-triggered reactions that occur between PS and the substances in its vicinity.[3,4] Specifically, type I reaction involves either hydrogen atom abstraction or electron transfer, ultimately leading to the formation of radicals and hydrogen peroxide (H_2O_2) while type II leads to the generation of singlet oxygen ($^1O_2$) by energy transfer from the electronically excited triplet-state PS to the ground-state molecular oxygen ($^3O_2$).[3,4] Type II PDT is the dominant mechanism since most of PSs are type II.[3,4] Unfortunately, this dependency on the surrounding oxygen contradicts the inherent properties of tumour hypoxia.

Hypoxia is a salient and important feature found in the microenvironment of solid tumours due to the fast cancer cell proliferation and irregular angiogenesis.[5] The oxygen pressure typically falls below 10 mmHg in the hypoxic regions of the tumour in contrast to the 40–60 mmHg range found in most healthy tissues.[6] Consequently, since type II PDT is highly dependent on oxygen concentrations, the hypoxic tumour

[a] *ICGM, Univ Montpellier, CNRS, ENSCM, Montpellier, France. E-mail: sebastien.clement1@umontpellier.fr*
[b] *IBMM, Univ Montpellier, CNRS, ENSCM, Montpellier, France. E-mail: jean-yves.winum@umontpellier.fr*
[c] *Univ Angers, CNRS, MOLTECH-ANJOU, SFR MATRIX, F-49000 Angers, France*
[d] *NEUROFARBA Department, Pharmaceutical and Nutraceutical Section, University of Florence, Via U. Schiff 6, 50019 Sesto Fiorentino, Firenze, Italy*
[e] *Université de Lorraine, CNRS, LRGP, F-54000 Nancy, France*
[f] *Latvian Institute of Organic Synthesis, Aizkraukles 21, 1006, Riga, Latvia*

† Electronic supplementary information (ESI) available: Experimental section, optical properties, hCA inhibition assays, biological assays. See DOI: https://doi.org/10.1039/d3ma00926b

microenvironment not only hampers the PDT efficiency but also exacerbates the existing hypoxia by consuming oxygen and vascular closure.[7] Hypoxic cells respond to PDT-induced damages by activating signaling cascades mostly regulated by transcription factors HIFs (hypoxia-inducible factors 1 and 2, HIF-1/2) and by releasing pro-angiogenic growth factors which sustain survival, stimulate metastasis, invasiveness, and recurrence of tumour cells.[8,9] Several strategies, including the direct delivery of exogenous oxygen to the tumour or the generation of oxygen *in situ*, have been developed to partially alleviate tumour hypoxia.[10–13]

However, these methods provide only a temporary oxygen supply and often result in modest degradation of HIF-1, which can significantly compromise PDT effectiveness. Consequently, the inhibition of the HIF-1 signalling pathway has emerged as a promising approach to mitigate tumour hypoxia.

Human carbonic anhydrase IX (hCA IX) and another related isoform, *i.e.* hCA XII, are transmembrane proteins regulated by hypoxia-inducible factor (HIF) transcription factors, leading to their overexpression under hypoxic conditions.[14] These transmembrane isoforms hCA IX and hCA XII are members of the hCA family of zinc enzymes (CA, EC 4.2.1.1) which play a crucial role in regulating the pH balance within tumours, thereby contributing to the survival, proliferation, invasion, and metastasis of cancer cells.[15] The overexpression and extracellular location of the active site of hCA IX/hCA XII in hypoxic cancer cells offer potential as a target for delivering PS to cancer cells in PDT, with the aim of addressing the limitations associated with this treatment approach. In 2017, Jung *et al.* described the synthesis of a BODIPY-based PS featuring hCA IX inhibitor (CAi) acetazolamide (**AAZ**).[16] This PS, designed to specifically target hCA IX, exhibited significantly improved effectiveness in causing phototoxicity *in vitro* against the aggressive human breast cancer MDA-MB-231 cell line, both in standard culture and in a spheroid model. Moreover, its ability to suppress tumour growth *in vivo* was also demonstrated when tested on xenograft mice inoculated with MDA-MB-231 cells. Since this pioneering work, a series of CAi-PS systems including conjugated polymer,[17] metal organic framework,[18,19] porphyrins,[20–22] and metal complexes were developed.[23–26] We recently reviewed all these systems highlighting that a synergistic treatment that enhances the PDT effect against hypoxic cancer cells and reduces resistance can be achieved by combining a PS with a CAi.[27] Nevertheless, although these studies have yielded promising results thus far, it is worth noting that comprehensive inhibition studies against recombinant proteins such as hCA IX, and hCA XII, as well as the cytosolic off-targets hCA I and hCA II, have only rarely been carried out.[27]

Herein, we design a series of CAi-PS hybrid systems incorporating as CAi either a classical benzenesulfonamide chemotype, known to strongly inhibit hCA isoforms with high potency, or coumarin and sulfocoumarin-based moieties more selective for hCA IX and XII and compare them with respect to their carbonic anhydrase inhibition activities and phototoxic effect.[28–30] We opted to develop a metal-free PS based on the thiochromenocarbazole imide (TCI) core, derived from the *N*-annulation process of benzothioxanthene imide (BTI).[31] The selection of the TCI core was driven by the existence of a nitrogen-containing cycle, allowing for extra and orthogonal functionalization through *N*-alkylation. Furthermore, its intriguing photophysical attributes, such as a high fluorescence quantum yield and noteworthy spin–orbit coupling (SOC), can be finely adjusted depending on the nature of the substituent. Compared to the parent BTI, TCI was found to be able to generate singlet oxygen (Φ_Δ = 0.14 in CH_2Cl_2) due to increased intersystem crossing (ISC) transition.[31] To increase the singlet oxygen generation quantum yield, we decided to introduce a bromine substituent, a well-known strategy to achieve efficient singlet oxygen sensitizers due to SOC.[32] The synthesis, optical properties as well as detailed biological and PDT studies in a human breast adenocarcinoma (MDA-MB-231) cell line of this innovative CAi-TCI hybrid system were then investigated.

Results and discussion

Design and synthesis

The synthetic route to a series of TCI PS featuring CAis is illustrated in Scheme 1. This series of PSs was achieved by formation of a 1,2,3-triazole bridge between a carbonic anhydrase inhibitor (coumarin, benzenesulfonamide and sulfocoumarin) and TCI-based PS through a Cu(I)-catalyzed 1,3-dipolar cycloaddition. A TCI PS without hCA IX inhibitor **7** was also prepared from hex-1-yne serving as a control system (Scheme 1). Azido-functionalized TCI PS **3** was prepared in 68% yield by *N*-alkylation of TCI **1** with 2-[2-(2-azidoethoxy)ethoxy]ethyl 4-methylbenzenesulfonate **2** in THF at 85 °C in the presence of sodium hydride. The structure of TCI **3** was confirmed by IR spectroscopy by the strong asymmetric stretching frequency at 2111 cm^{-1} related to the azido group. High-resolution ESI-TOF mass spectrometry (positive mode) also revealed the presence of the pseudo-molecular ion $[M + H]^+$ at m/z = 622.1105 Da in agreement with the calculated one (calcd m/z = 622.1118 Da).

Alkyne-substituted carbonic anhydrase inhibitors were then grafted to azido-functionalized TCI **3** *via* a copper catalysed azide alkyne cycloaddition reaction in a mixture of THF–H_2O, affording the TCI-CAi-based PSs **4–6** with yields ranging from 60% to 84%. A control system without a CA inhibitor was also elaborated through the reaction of TCI **3** with hex-1-yne (Scheme 1). The disappearance of the strong N_3 stretching bands in the ATR-FTIR spectra of TCIs **4–7** confirmed that the cycloaddition occurred. The formation of the triazole ring was also corroborated by ^{1}H NMR spectroscopy and by the presence of an additional singlet between 7.20 and 7.90 ppm.

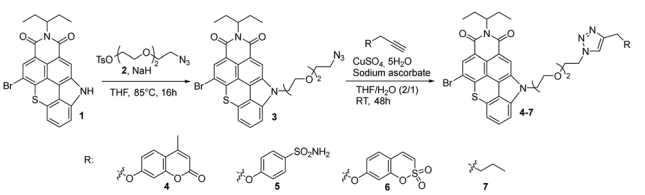

Scheme 1 Synthetic route to CAi-based TCIs.

Additional signals corresponding to CAi moieties were also observed: two signals at 2.40 ppm (CH_3) and 6.23 ppm (hydrogen close to the carbonyl) for the coumarin-based TCI **4**, two doublets at 6.95 ppm and 7.79 ppm (hydrogens of the phenyl group) for the benzenesulfonamide-based TCI **5**, signals between 6.75 and 7 ppm (aromatic hydrogens) for the sulfocoumarin-based TCI **6** and finally, signals corresponding to the CH_2 and CH_3 groups between 0.90 and 2.26 ppm for TCI **7**. Finally, the presence of monocations $[M + H]^+$ was also observed in the high-resolution ESI-TOF mass spectra (positive mode) of all CAi-TCI PSs **4–6** as well as the control PS **7**.

Optical properties

All molecules were studied in diluted DMF solutions and their absorption, maximum emission wavelength, fluorescence quantum yield and lifetime were systematically studied. The absorption and emission spectra of CAi-TCI **4** are depicted in Fig. 1 as an example. All the CAi-TCI hybrid systems exhibit two broad absorption bands centered at around 410 nm and 480 nm corresponding to the absorption of the TCI central core. These CAi-TCI hybrid systems exhibit a broad emission band at 532 nm with moderate Stokes shift (~50 nm) and fluorescence quantum yields between 0.13 and 0.20 using rose bengal as a reference (Φ_F = 0.11 in EtOH).[33]

The ability of PSs **4–7** to generate $^1O_2$ was then evaluated by monitoring its photoluminescence (PL) at 1270 nm in aerated DMF using rose bengal as a reference (Φ_Δ = 0.40).[33] As shown in Table 1, the nature of CAi had very little effect on the production of $^1O_2$ with a $^1O_2$ yield between 0.31–0.40 for all TCIs **4**, **6**, **7** whereas in the case of **5**, a little lower $^1O_2$ quantum yield is noticed. These yields are in the same range as that of rose bengal.[34] Indeed, the presence of a halogen substituent, namely bromine, on the TCI core enables efficient singlet oxygen generation due to increased singlet-to-triplet inter-system crossing (ISC) owing to the so-called heavy atom effect.[31]

Carbonic anhydrase inhibition assays

The CAi-TCI hybrid systems **4–6** as well as TCI PS without hCA IX inhibitor **7** were subsequently assessed for their inhibitory activity against carbonic anhydrases, using a stopped-flow assay method. Four clinically relevant human isoforms were investigated including the two cytosolic off-targets, hCA I and hCA II, along with two tumour-associated membrane-bound isoforms, hCA IX and hCA XII. The clinically used acetazolamide (**AAZ**) served as a reference drug (Table 2). As anticipated, the negative control **7**, which lacks a pharmacophoric CA inhibitory moiety, exhibited no inhibitory activity (K_i > 100 μM) against the four tested isoforms. When compared to the standard drug **AAZ**, which effectively inhibits all four CA isoforms considered in this study, analogues **4**, **5** and **6** exhibited lower effectiveness as hCA IX and XII inhibitors.

However, derivatives **4** and **6** displayed strong selectivity, as neither of them inhibited the cytosolic off-targets hCA I and hCA II. Specifically, coumarin derivative **4** and sulfocoumarin derivative **6** demonstrated identical activity profiles against the membrane-bound isoforms, with an inhibitory activity against hCA IX at 86.2 and 76.9 nM, respectively, and a slightly improved inhibitory activity against hCA XII, with K_i values of 45.3 and 48.2 nM, respectively. Although compound **5** displayed one of the best inhibition values against hCA IX and hCA XII, with inhibition constants of 42.9 and 21.3 nM, respectively, it exhibited the same inhibitory profile against hCA I and hCA II. The lack of selectivity of benzenesulfonamide towards the different CA isoforms is well-known[28–30] and is due to the lack of additional interactions with hydrophobic and/or hydrophilic residues in the region of the active site, which influences the

Table 1 Summary of the main spectroscopic and photophysical data for all studied CAi-TCI hybrid systems

Compounds	λ_{abs} (nm)	ε (L mol^{-1} cm^{-1})	λ_{em} (nm)	Φ_F[a]	τ_{obs} (ns)	Φ_Δ[ab]
4	410	42 000	532	0.20	7.6	0.36
	481	47 600				
5	412	44 700	532	0.18	7.0	0.25
	483	50 000				
6	413	39 800	532	0.13	9.8	0.31
	483	43 500				
7	410	51 500	532	0.18	6.7	0.39
	480	56 100				

[a] Rose bengal was used as a reference both for determining fluorescence quantum yields and $^1O_2$ generation efficiency. [b] $^1O_2$ generation efficiency.

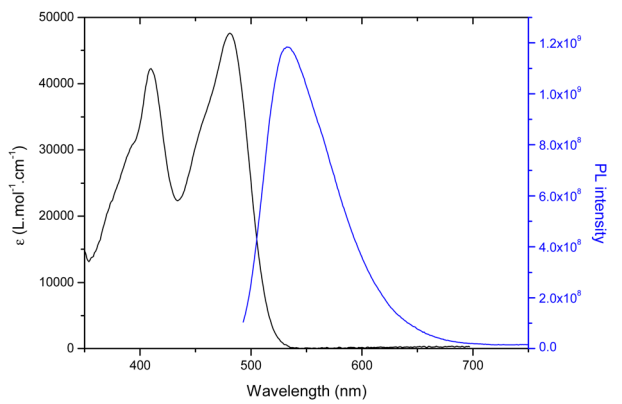

Fig. 1 UV-visible absorption (black) and emission spectra (blue) of CAi-TCI **4** in DMF (C = 1.5 × 10^{-5} mol L^{-1}, λ_{exc} = 435 nm).

Table 2 Inhibitory activity of PSs **4–7** against hCA I, hCA II, hCA IX and hCA XII using acetazolamide (**AAZ**) as reference drug

	K_i[a] (nM)			
	Cytosolic		Membrane-bound	
Compounds	hCA I	hCA II	hCA IX	hCA XII
4	>100 μM	>100 μM	86.2	45.3
5	89.5	28.7	42.9	21.3
6	>100 μM	>100 μM	76.9	48.2
7	>100 μM	>100 μM	>100 μM	>100 μM
AAZ	250	12	25	5.7

[a] Mean from three different measurements by a stopped flow technique (errors were in the range of 5–10% of the reported values).

inhibitor binding but also, the selectivity.[35,36] Given the absence of selectivity exhibited by compound **5**, we considered only the selective inhibitors **4** and **6**, along with the negative control **7**, in the biological studies.

Biological studies *in vitro*

The biological potential of **4**, **6** and **7** was studied both *in vitro* and *in vivo*. First, human breast cancer cell line (MDA-MB-231) was used to establish the dark cytotoxicity of these three compounds. To achieve this goal and in order to reduce the risk of precipitation due to solubilization of compounds in aqueous media, the compounds were first dissolved in DMSO followed by 10-fold dilutions in culture media. Fig. 2(A) describes the cell viability after 72 h of incubation with increasing concentrations of **4**, **6** and **7** from 0.1 to 100 μg mL^{-1}, corresponding to 0.12 to 142.21 μM (Fig. S24 in the ESI†). As observed, **4** and **6** exhibit relatively low toxicity in the studied condition while **7** is strongly toxic from 5 μg mL^{-1} (7.11 μM). In order to clearly demonstrate a PDT effect without any dark toxicity background, we performed the PDT experiments by incubating cells with only 0.5 μg mL^{-1} compound (Fig. 2(B)).

For this, MDA-MB-231 cells were incubated 24 h with 0.5 μg mL^{-1} compound and excited during 30 s with a blue LED source (470 ± 22 nm). Two days later, living cells were quantified and Fig. 2(B) showed that compounds **4**, **6** and **7** are very efficient in killing cancer cells by PDT with 75%, 57% and 86% of cell death induced by light excitation, respectively. Then, we decided to analyse the imaging potential of such compounds by incubating cells with the ligands at 10 μg mL^{-1} for 24 h. Fig. 2(C) highlights the strong fluorescence of compounds **4** and **7** and the localisation inside the cells, which suggests their potential for imaging of living cells.

These data demonstrate that **4** exhibits a low toxic level without specific excitation, a strong PDT and imaging potential. Compound **6** is not toxic in the studied conditions without excitation, but it is less efficient in PDT and particularly in imaging. Finally, while compound **7** may be deemed the most effective choice for imaging and PDT, its notable high toxicity above 5 μg mL^{-1} stems from its lack of specificity, as it can be internalized by all cells owing to its lipophilic properties.

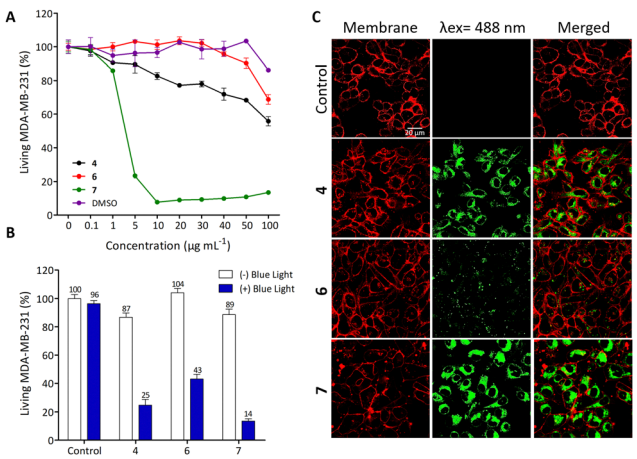

Fig. 2 (A) Toxicity study on the human breast cancer cell line (MDA-MB 231) incubated 3 days with increasing concentrations of **4**, **6**, **7** and the corresponding volume of the vehicle (DMSO). Values are mean ± SEM of three experiments. (B) Phototoxic effect of **4**, **6**, **7** on MDA-MB 231 cells incubated with 0.5 μg mL^{-1} of compounds for 24 h then exposed to blue light at 469–494 nm for 30 seconds using EVOS. Cell viability was quantified after 48 h. Results are presented as mean ± SEM of three experiments. (C) Confocal microscopy imaging of living MDA-MB-231 cells incubated with 10 μg mL^{-1} of **4**, **6**, **7** for 24 h using confocal microscopy LSM780.

Biological studies *in vivo*

These highly encouraging results on cells led us to test their effectiveness *in vivo*, on zebrafish embryos. This is a particularly well-suited substitute animal model for small mammals to study biocompatibility, PDT, and imaging.[37,38] We first injected the three compounds into the intravenous system of embryos. More precisely, 10 nL of **4**, **6** and **7** at a concentration of 1 mg mL^{-1} in 5% glucose were injected in the tail vein of embryos at 72 hours post-fertilization (hpf). If we consider a total blood volume of around 80 nL for a 72 hpf embryo,[39] the injection of 10 nL at 1 mg mL^{-1} allows to reach a final concentration of around 111 μg mL^{-1} (Fig. 3). As observed *in vitro*, at first sight, all compounds were luminescence and very well dispersed in the embryos, suggesting a good bioavailability, but analogue **6** was the least fluorescent. **4** was also well-dispersed and particularly luminescence when observed under the same condition of **6**, that is 3 hours after injection and using a laser power of 30%.

Finally, the negative control **7** exhibiting a tremendous brightness is visualized at only 1% laser power and immediately after injection because embryos died in the minutes following the injection. Taking all these results into account, we concluded that compound **4** was the most effective in terms of imaging and PDT, while maintaining a high level of safety. So, we decided to study its PDT activity *in vivo*. For this, MDA-MB-231 cells stably expressing red fluorescece protein were injected in the yolk of 30 hpf embryos.

These MDA-MB-231 cells were previously treated (or not) with 10 μg mL^{-1} of compound **4** for 24 h (Fig. 4). Twenty-four hours after cell injection, embryos were imaged then, exposed to blue light for 2 min. One day later, embryos were imaged again to monitor the xenograft growth. By quantifying the fluorescence

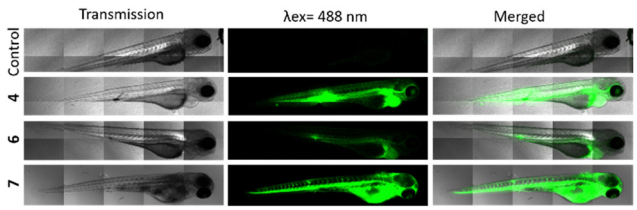

Fig. 3 Casper zebrafish embryos at 72 hours post-fertilization (hpf) were injected with 10 nL of **4**, **6**, **7** at a concentration of 1 mg mL^{-1} in 5% glucose (final concentration ~ 111 μg mL^{-1}). Embryos injected with **4** and **6** were observed with LSM880 (laser power 30%) 3 h post-injection. Embryos injected with **7** were observed with LSM880 (laser power 1%) immediately after injection.

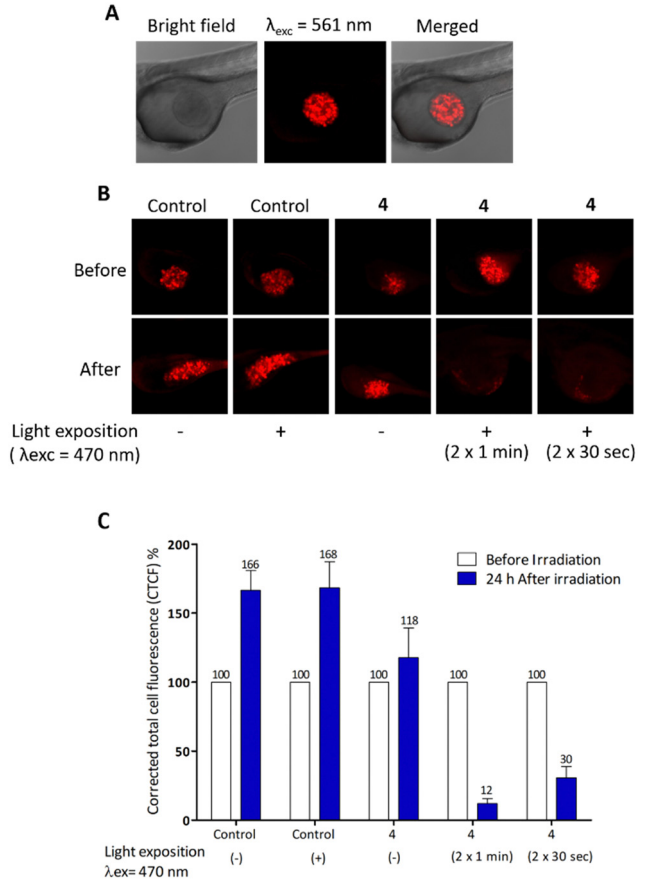

Fig. 4 (A) Casper zebrafish embryos at 30 hpf were used for the microinjection of red fluorescence cells (MDA-MB-231-Luc-RFP) previously incubated (or not) with **4**. Each embryo received 10 nL of cell suspension in the yolk. Injected Casper embryos with cells without **4** were used as controls. (B) Twenty-four hours after injection, the embryos were exposed or not to light excitation (470 nm) (n = 10/group) during 2 or 1 min (λ_{ex} = 470 ± 22 nm, 9.41 J cm^{-2}). (C) The fluorescence intensity of the xenografts before and 24 h after irradiation was quantified using the ImageJ program. The corrected total cell fluorescence (CTCF) was calculated as CTCF = integrated density − (area of selected cell × mean fluorescence of background readings) and the tumour regression (%) was calculated considering the fluorescence intensity value of each embryo before irradiation is 100%.

intensity of the xenograft before and after light exposure, results (Fig. 4) show the high efficiency of compound **4** in eradicating the tumours.

Conclusions

In summary, we successfully designed and synthesized thiochromenocarbazole imide derivatives incorporating carbonic anhydrase inhibitor moiety. Among the three CAi-TCI hybrid systems that were the subject of biological assays, compound **4**, featuring the selective hCA IX/hCA XII coumarin inhibitor, displayed low dark toxicity and exhibited robust imaging and PDT effects both *in vitro* and *in vivo*. Interestingly, the negative-control compound **7**, lacking pharmacophoric scaffold able to inhibit CA, surprisingly demonstrated significant imaging and PDT effects, albeit with high toxicity. The high lipophilicity of this non-targeted photosensitizer may account for its effectiveness, as it can readily penetrate various cell types, thereby explaining its significant toxicity. This underscores the importance of focusing on therapeutic targets, such as relevant carbonic anhydrase isoforms, to address this issue. Altogether, this study provides a valuable resource for the study of innovative photosensitizers linked to selective carbonic anhydrase inhibitors, with potential applications in imaging and phototherapy.

Data availability

All of the additional information and experimental data are provided in the ESI.†

Author contributions

Merabti A: methodology, investigation; Puchan Sanchez D: methodology, investigation; Nocentini A: methodology, investigation; Ali L. M. A.: methodology, investigation; Nguyen C: methodology, investigation; Durand D: methodology, investigation; Hamon K: methodology, investigation; Ghanem T: methodology, investigation; Arnoux P: methodology, investigation; Josse P: methodology, investigation; Frochot C: formal analysis, review & editing; Zalubovskis R: methodology, investigation; Richeter S: methodology, investigation; Gary-Bobo: formal analysis, writing – review & editing; Supuran CT: formal analysis, review & editing; Cabanetos C: formal analysis, review & editing; Winum J-Y: formal analysis, conceptualization, supervision, writing – review & editing; Clément S: formal analysis, conceptualization, supervision, writing – review & editing.

Conflicts of interest

There are no conflicts to declare.

Acknowledgements

The authors are grateful to the University of Montpellier, the CNRS and the French Ministry of Research for financial support. The work is also partly supported by Ligue contre le Cancer funding to SC and JYW. A. M. thanks the Algerian Ministry of Education and Research for her PhD grant. We acknowledge the ZeNeuro platform (Inserm U1198), especially Nicolas Cubedo, and the imaging facility ''Montpellier Ressources Imagerie'' (MRI), member of the national infrastructure France-BioImaging supported by the French National Research Agency (ANR\u000210-INBS-04, ''Investments for the future''). The ANR is also acknowledged for the financial support of BTXI-Apogee (ANR-20-CE05-0029) used for the development and synthesis of TCI precursors.

Notes and references

1 W. Jiang, M. Liang, Q. Lei, G. Li and S. Wu, *Cancers*, 2023, **15**(3), 585.
2 H. O. Alsaab, M. S. Alghamdi, A. S. Alotaibi, R. Alzhrani, F. Alwuthaynani, Y. S. Althobaiti, A. H. Almalki, S. Sau and A. K. Iyer, *Cancers*, 2020, **12**(10), 2793.
3 J. P. Celli, B. Q. Spring, I. Rizvi, C. L. Evans, K. S. Samkoe, S. Verma, B. W. Pogue and T. Hasan, *Chem. Rev.*, 2010, **110**(5), 2795.
4 S. Kwiatkowski, B. Knap, D. Przystupski, J. Saczko, E. Kedzierska, K. Knap-Czop, J. Kotlinska, O. Michel, K. Kotowski and J. Kulbacka, *Biomed. Pharmacother.*, 2018, **106**, 1098.
5 A. Challapalli, L. Carroll and E. O. Aboagye, *Clin. Transl. Imaging*, 2017, **5**(3), 225.
6 J. M. Brown and W. R. Wilson, *Nat. Rev. Cancer*, 2004, **6**, 437.
7 K. R. Atkuri, L. A. Herzenberg, A.-K. Niemi and T. Cowan, *Proc. Natl. Acad. Sci. U. S. A.*, 2007, **104**, 4547.
8 V. Petrova, M. Annicchiarico-Petruzzelli, G. Melino and I. Amelio, *Oncogenesis*, 2018, **7**(1), 10.
9 G. Chen, K. Wu, H. Li, D. Xia and T. He, *Front. Oncol.*, 2022, **12**, 961637.
10 L. Larue, B. Myrzakhmetov, A. Ben-Mihoub, A. Moussaron, N. Thomas, P. Arnoux, F. Baros, R. Vanderesse, S. Acherar and C. Frochot, *Pharmaceuticals*, 2019, **12**(4), 163.
11 Y. Wan, L.-H. Fu, C. Li, J. Lin and P. Huang, *Adv. Mater.*, 2021, **33**(48), e2103978.
12 C. Zhang, X. Hu, L. Jin, L. Lin, H. Lin, Z. Yang and W. Huang, *Adv. Healthcare Mater.*, 2023, **12**(24), e2300530.
13 N. Kwon, T. Guo, Z. Liu and J. Yoon, *Angew. Chem., Int. Ed.*, 2018, **57**(36), 11522.
14 C. T. Supuran, *Bioorg. Med. Chem. Lett.*, 2023, **93**, 129411.
15 S. Kalinin, A. Malkova, T. Sharonova, V. Sharoyko, A. Bunev, C. T. Supuran and M. Krasavin, *Int. J. Mol. Sci.*, 2021, **22**(24), 13405.
16 H. S. Jung, J. Han, H. Shi, S. Koo, H. Singh, H.-J. Kim, J. L. Sessler, J. Y. Lee, J.-H. Kim and J. S. Kim, *J. Am. Chem. Soc.*, 2017, **139**(22), 7595.
17 Y. Jiang, J. Li, Z. Zeng, C. Xie, Y. Lyu and K. Pu, *Angew. Chem., Int. Ed.*, 2019, **58**(24), 8161.
18 W. Zhu, Y. Liu, Z. Yang, L. Zhang, L. Xiao, P. Liu, J. Wang, C. Yi, Z. Xu and J. Ren, *J. Mater. Chem. B*, 2018, **6**, 265.
19 W. Zhu, L. Zhang, Z. Yang, P. Liu, J. Wang, J. Cao, A. Shen, Z. Xu and J. Wang, *Chem. Eng. J.*, 2019, **358**, 969.
20 G.-L. Fan, P. Yuan, F.-A. Deng, L.-S. Liu, Y.-L. Miao, C. Wang, X.-Z. Qiu, X.-Y. Yu, H. Cheng and S.-Y. Li, *ACS Appl. Bio. Mater.*, 2020, **3**(9), 6124.
21 F. Wang, T. X. Meerovich, F. Hong, Z.-L. Chen and Y.-J. Yan, *Dyes Pigm.*, 2022, **203**, 110328.
22 A. Merabti, M. Roger, C. Nguyen, A. Nocentini, P. Gerbier, S. Richeter, M. Gary-Bobo, C. T. Supuran, S. Clément and J.-Y. Winum, *Eur. J. Org. Chem.*, 2022, e202101538.
23 X. Su, W.-J. Wang, Q. Cao, H. Zhang, B. Liu, Y. Ling, X. Zhou and Z.-W. Mao, *Angew. Chem., Int. Ed.*, 2022, **61**, e202115800.
24 P. Kumar, P. Singh, S. Saren, J. Sayala, S. Sivakumar and A. K. Patra, *Dalton Trans.*, 2022, **51**, 18416.
25 L. Hao, J. Wang, Z.-Y. Pan, Z.-W. Mao and C.-P. Tan, *Chem. Commun.*, 2022, **58**, 8069.
26 H. S. Jung, S. Koo, M. Won, S. An, H. Park, J. L. Sessler, J. Han and J. S. Kim, *Chem. Sci.*, 2023, **14**, 1808.
27 A. Merabti, S. Richeter, C. T. Supuran, S. Clément and J.-Y. Winum, *Expert Opin. Ther. Targets*, 2023, **27**(9), 817, DOI: **10.1080/14728222.2023.2255380**.
28 A. Angeli, F. Carta, A. Nocentini, J. Y. Winum, R. Zalubovskis, A. Akdemir, V. Onnis, W. M. Eldehna, C. Capasso, G. De Simone, S. M. Monti, S. Carradori, W. A. Donald, S. Dedhar and C. T. Supuran, *Metabolites*, 2020, **10**(10), 412.
29 C. B. Mishra, M. Tiwari and C. T. Supuran, *Med. Res. Rev.*, 2020, **40**(6), 2485.
30 C. T. Supuran, *Expert Opin. Ther. Pat.*, 2023, **33**(11), 701, DOI: **10.1080/13543776.2023.2245971**.
31 L. Abad Galán, J. M. Andrés Castán, C. Dalinot, P. Simón Marqués, P. Blanchard, O. Maury, C. Cabanetos, T. Le Bahers and C. Monnereau, *Phys. Chem. Chem. Phys.*, 2020, **22**, 12373.
32 J. María Andrés Castán, C. Amruth, P. Josse, L. Abad Galan, P. Simón Marqués, M. Allain, O. Maury, T. Le Bahers, P. Blanchard, C. Monnereau, G. C. Welch and C. Cabanetos, *Mater. Chem. Front.*, 2022, **6**, 1912.
33 P. G. Seybold, M. Gouterman and J. Callis, *Photochem. Photobiol.*, 1969, **9**(4), 229.
34 R. W. Redmond and J. N. Gamlin, *Photochem. Photobiol.*, 1999, **70**(4), 391.
35 V. Alterio, A. Di Fiore, K. D'Ambrosio, C. T. Supuran and G. De Simone, *Chem. Rev.*, 2012, **112**(8), 4421.
36 M. A. Pinard, B. Mahon and R. McKenna, *BioMed Res. Int.*, 2015, **2015**, 15.
37 Z. Chen, S. Pascal, M. Daurat, L. Lichon, C. Nguyen, A. Godefroy, D. Durand, L. M. A. Ali, N. Bettache, M. Gary-Bobo, P. Arnoux, J.-F. Longevial, A. D'Aléo, G. Marchand, D. Jacquemin and O. Siri, *ACS Appl. Mater. Interfaces*, 2021, **13**(26), 30337.
38 N. Hamon, A. Roux, M. Beyler, J.-C. Mulatier, C. Andraud, C. Nguyen, M. Maynadier, N. Bettache, A. Duperray, A. Grichine, S. Brasselet, M. Gary-Bobo, O. Maury and R. Tripier, *J. Am. Chem. Soc.*, 2020, **142**(22), 10184.
39 E. Cörek, G. Rodgers, S. Siegrist, T. Einfalt, P. Detampel, C. M. Schlepütz, S. Sieber, P. Fluder, G. Schulz, H. Unterweger, C. Alexiou, B. Müller, M. Puchkov and J. Huwyler, *Small*, 2020, **16**(31), 2000746.